Journal Name

Dynamic Article Links ►

Cite this: DOI: 10.1039/c0xx00000x

www.rsc.org/xxxxxx

ARTICLE TYPE

Quantitative understanding of thermal stability of α"-$Fe_{16}N_2$

Shinpei Yamamoto,[*,a] Ruwan Gallage,[a,b] Yasunobu Ogata,[c] Yoshihiro Kusano,[d] Naoya Kobayashi,[b,e] Tomoyuki Ogawa,[c] Naoaki Hayashi,[a] Kaori Kohara,[a,b] Migaku Takahashi[f] and Mikio Takano[a]

Received (in XXX, XXX) Xth XXXXXXXXX 20XX, Accepted Xth XXXXXXXXX 20XX

DOI: 10.1039/b000000x

Thermal stability of α"-$Fe_{16}N_2$, which attracts much interest because of its superior magnetic properties featuring a large magnetocrystalline anisotropy (K_u ~ 1 × 10^7 erg/cm^3) and saturation magnetization (M_s ~ 234 emu/g), though unfortunately thermally unstable, has been *quantitatively* studied.

α"-$Fe_{16}N_2$ is a meta-stable iron nitride with body-centered tetragonal (bct) structure, which is essentially α-Fe containing the nitrogen atoms ordered on interstitial sites. This material has attracted much interest since the first report of a 'giant' magnetic moment in it.[1] Although the formation of this phase was already reported in 1951,[2] it has been difficult to obtain monophasic samples, and this has made the reported saturation magnetization (M_s) highly scattered.[3] We recently have succeeded in preparing high-purity powdered samples in a large size of 10 g/batch and reported that the M_s and the uniaxial magnetocrystalline anisotropy, K_u, were as high as 234 emu/g and *ca.* 1 × 10^7 erg/cm^3, respectively at 5 K.[4] These values are in good agreement with those determined by M. Takahashi *et al.* using thin films which were the best samples at that time[3a] and also with the estimation based on first principle calculations.[6] Potential use of these superior properties for magnetic recording and microwave absorption has attracted much attention.[7] Recently, another possible application as a rare earth-free permanent magnet has emerged because of the rare-earth crisis.[8,9]

Stability at elevated temperatures is a key issue in both fabrication and use. Especially because the present material is known to be meta-stable and *quantitative* understanding of thermal decomposition processes is highly needed. However, difficulties in obtaining monophasic samples have made even the reported decomposition temperature highly scattered from about 473 to 673 K.[2,3f,10-13] Furthermore, relevant studies have mostly done indirectly through measurements of magnetization that decreases as the volume fraction of α"-$Fe_{16}N_2$ decreases. Another problem is the fact that thin films grown on substrates or precipitates embedded in massive matrices have been used as samples, the decomposition behaviour of which may well be affected by electronic and structural constraints imposed by the substrates or the matrices. Here, we report a *quantitative* study using free-standing, high-purity nanoparticles subjected to temperature- and time-dependent powder X-ray diffraction (XRD) measurements under inert gaseous conditions (N_2 and Ar). A kinetic description of the decomposition processes will open ways to new applications such as a car motor magnet where higher working temperatures are necessary.

The α"-$Fe_{16}N_2$ nanoparticles (NPs) used in this study were prepared in two steps, oxide-to-metal reduction in a H_2 stream and subsequent metal-to-nitride conversion using an NH_3 stream, which may be expressed α-Fe_2O_3 → α-Fe → α"-$Fe_{16}N_2$.[5] In the starting powder no crystalline impurity phases such as γ'-Fe_4N, ε-Fe_3N, α-Fe and iron oxides were detected by XRD (see Figure S1 in the Electronic Supplementary Information (ESI)). However, the presence of *ca.* 9 % of an amorphous phase, which we suppose to be insufficiently nitrided and consequently amorphized particles, α-FeN_x (x < 0.125), was suggested by the Rietveld analysis of the XRD result (see Figure S2(a) in the ESI). The average crystallite size of α"- $Fe_{16}N_2$ NPs estimated by using the Scherrer formula was 29.6 nm. For the decomposition studies, the α"-$Fe_{16}N_2$ NPs were sealed in borosilicate capillaries under N_2 or Ar and immersed in preheated oil baths (473, 493, 503 and 513 K) for certain periods of time (t). Temperature- and time-dependent XRD patterns taken under N_2 are shown in Figure S3 in ESI. Upon increment of the heating time (t), α"-$Fe_{16}N_2$ decreases while α-Fe and γ'-Fe_4N appear and increase. No other crystalline phases were detected, while the intensity of the broad peak assigned to an amorphous phase was doubled in an early stage but was soon decreased to the initial level, suggesting the presence of interfacial regions containing disordered nitrogen atoms.

In order to quantitatively estimate decomposition kinetics, the relative weight fractions of α"-$Fe_{16}N_2$ (w_{Fe16N2}), α-Fe (w_{Fe}), γ'-Fe_4N (w_{Fe4N}) and the amorphous phase (w_{amor}) were estimated by the Rietveld analyses (also see Figure S4 and Table S1 in the ESI). The fraction of decomposition, D, can be expressed as:

$$D = 1 - w_{Fe16N2}(T, t) / w_{Fe16N2}(300, 0) \quad (1)$$

where $w_{Fe16N2}(300, 0)$ and $w_{Fe16N2}(T, t)$ represent the fraction of α"-$Fe_{16}N_2$ before (= 0.9056) and after a heat-treatment at T [K] for a certain period of time (t), respectively. Fig. 1a ~ d show the time dependence of decomposition at various temperatures. These are all well represented by the first order reaction model formulated as

$$D = 1 - \exp(-k_{app} \cdot t) \quad (2)$$

where k_{app} is an apparent rate constant.[14] Summarized in Fig. 1e are the D vs. $t_{1/2}$ relation measured at different temperatures and atmospheres, where $t_{1/2}$ is the time when D reaches 0.5 (see Table S2 in the ESI). All the experimental data fall into a single curve, revealing that the decomposition mechanism remains the same

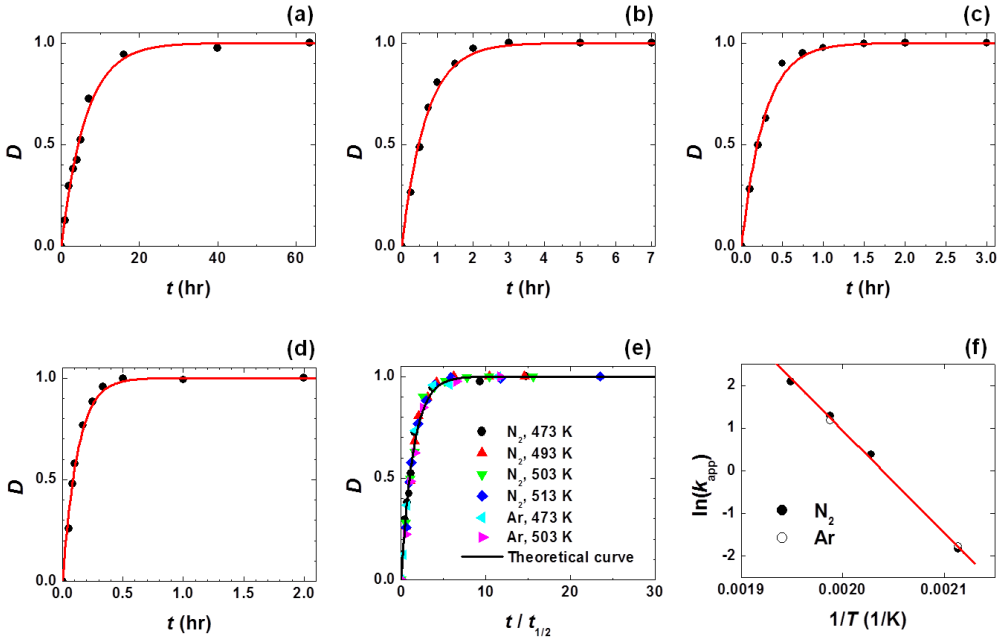

Fig. 1 Fraction of decomposed α"-$Fe_{16}N_2$ (D) plotted against heating time (t) at (a) 473 K, (b) 493 K, (c) 503 K, and (d) 513 K under N_2. The solid symbols and red lines represent the experimental data and the least-squares fittings using eq.(2), respectively. (e) Plots of D vs. $t/t_{1/2}$, where those collected under Ar are included together. The solid symbols and black line represent the experimental data and theoretical curve, respectively. Concerning the definition of $t/t_{1/2}$, see the text. (f) Plots of $\ln(k_{app})$ *vs.* inverse temperature ($1/T$). The symbols and the red line represent the experimental data and the least-squares fitting, respectively.

irrespective of temperature and atmosphere. Furthermore, it is worth noting that even the raw experimental data collected under N_2 and Ar fall into the same D vs. t curve, revealing that not only the basic mechanism but also the kinetic parameters are *quantitatively* the same for these atmospheres (see Figure S5 and S6 in the ESI).

Thermal decomposition is a thermally activated process, and k_{app} can be expressed as below using an Arrhenius-type equation:

$$k_{app} = k_0 \cdot \exp(-\Delta E_{app}/RT) \quad (3)$$

where k_0, ΔE_{app}, R, and T are the frequency factor, apparent activation energy, gas constant and absolute temperature, respectively. From the so-called Arrhenius plot of $\ln(k_{app})$ *vs.* $1/T$ shown in Fig. 1f, k_0 and ΔE_{app} have been deduced to be $e^{48.9}$ [1/h] and 199 [kJ/mol], respectively. Two previous works done on α"-$Fe_{16}N_2$ precipitates embedded in bulk Fe-N alloy matrices reported largely different values.[12] Predicting the thermal stability of α"-$Fe_{16}N_2$ in an inert atmosphere *quantitatively* based on the present study, as shown in Fig.2 , α"-$Fe_{16}N_2$ devices should be kept below about 355 K in order to maintain their performance better than 99 % for 100 years, for instance. The time allowance *vs.* temperature relation shown in Figure S7 in the ESI must be *quantitatively* useful for development of device fabrication processes and others.

Fig. 3 shows plots of w_{Fe4N} *vs.* w_{Fe}. All of the data points fall into the single line of $w_{Fe4N} = 1.06\ w_{Fe}$, revealing that α"-$Fe_{16}N_2$ thermally decomposes into a 4:1 molar mixture of α-Fe and γ'-Fe_4N without releasing nitrogen into the atmosphere. The increment of w_{Fe4N} and w_{Fe} ceases at about 0.45 due to the presence of the amorphous phase ($w_{amor} \sim 0.1$). It is worth noting that, upon heat-treatment, the amorphous phase first increases to $w_{amor} \sim 0.22$ and subsequently decreases to the initial level of ~ 0.1 (see Figure S4(b) in the ESI). This behavior can be understood by assuming the existence of two amorphous phases: one is that already contained in the pristine sample which remains intact during heat-treatment (~ 0.1). The other arises from insufficient atomic rearrangements during thermal decomposition, which is responsible for the initial increment and the subsequent decrement.

Another important experimental fact is that evolution of nitrogen gas during decomposition was not detected at all by mass spectroscopic analyses done in an Ar stream (see Figure S8 in the ESI). Together with the XRD data, the thermal decomposition reaction can thus be exactly expressed as a solely intra-solid atomic rearrangement:

$$\alpha\text{"-}Fe_{16}N_2 \rightarrow 8(\alpha\text{-Fe}) + 2(\gamma\text{'-}Fe_4N) \quad (4)$$

The observed ΔE_{app} of 199 [kJ/mol] is closer to the activation energy for the diffusion of iron atoms in bcc-iron, 250 [kJ/mol][15], rather than to the activation energy for the diffusion of nitrogen atoms in Fe-N alloys, 90 [kJ/mol][16]. Most probably the energy-consuming iron diffusion is the initial step of the reaction that is indispensably necessary to make space for nitrogen to be condensed to form γ'-Fe_4N. To enhance the practical stability of α"-$Fe_{16}N_2$ it is necessary to suppress the formation of γ'-Fe_4N. Doping of Ti, Cr, Al and Mn (3-15 %, nominal), known to suppress the formation of γ'-Fe_4N in Fe-N alloys,[17] may be useful.

In conclusion, we have successfully revealed the thermal decomposition process and kinetics of α"-$Fe_{16}N_2$ under inert gaseous conditions. The decomposition mechanism is solely intra-solid atomic rearrangements. The decomposition products are α-Fe and γ'-Fe_4N mixed at 4:1 (molar ratio), and the process

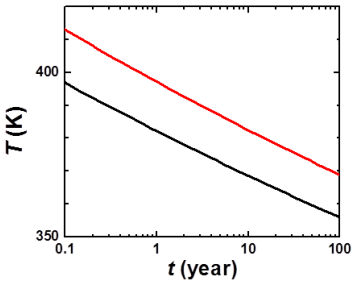

Fig. 2 Thermal stability of α"-$Fe_{16}N_2$; the upper limit to which 99 % and 90 % of α"-$Fe_{16}N_2$ remain intact are shown in the black and red lines, respectively.

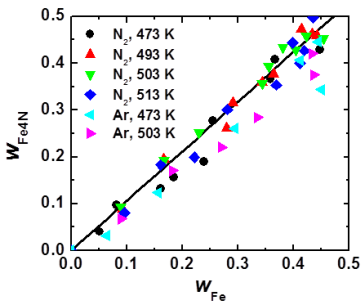

Fig. 3 Plots of w_{Fe4N} *vs.* w_{Fe}. The solid line represents the $w_{Fe4N} = 1.06\ w_{Fe}$ relation.

can be well represented by the first order reaction model: $D = 1 - \exp(-k_{app} \cdot t)$, where k_{app} [1/h] = $\exp(48.9 - 23.9 \times 10^3/T)$. The formation of γ'-$Fe_4N$ with a higher thermal stability is responsible for the irreversible nature of the thermal decomposition processes. To enhance the thermal stability of α"-$Fe_{16}N_2$, it is indispensably necessary to somehow suppress the formation of the γ'-phase. Quantitative understanding of thermal stability of α"-$Fe_{16}N_2$ given in this work will open ways to new applications such as a car motor magnet where higher working temperatures are necessary.

This work was partly supported by the Research and Development of Alternative New Permanent Magnetic Materials to Nd-Fe-B Magnets Project from NEDO of Japan and MEXT KAKENHI (Nos 20104006 and 21226007).

Notes and references

[a] *Institute for Integrated Cell-Material Sciences (iCeMS), Kyoto University, Yoshida Ushinomiya-cho, Sakyo-ku, Kyoto 606-8501, Japan*
[b] *Toda Kogyo Corporation, 1-4 Meijishinkai, Otake, Hiroshima 739-0652, Japan*
[c] *Department of Electronic Engineering, Graduate School of Engineering, Tohoku University, 6-6-05 Aza-Aoba, Aramaki, Aoba-ku, Sendai 980-8579, Japan*
[d] *Department of Fine & Applied Arts, Kurashiki University of Science and the Arts, 2640 Nishinoura, Tsurajima-cho, Kurashiki-shi, Okayama 712-8505, Japan*
[e] *T&T Innovations Inc., 1-4 Meijishinkai, Otake, Hiroshima 739-0652, Japan*
[f] *New Industry Creation Hatchery Center (NICHe), Tohoku University, 6-6-10 Aza-Aoba, Aramaki, Aoba-ku, Sendai 980-8579, Japan*

† Electronic Supplementary Information (ESI) available: [details of experimental, XRD pattern of the pristine α"-$Fe_{16}N_2$ nanoparticles and an empty borosilicate capillary (Figure S1), typical examples of the Rietveld analyses (Figure S2), XRD patterns of the samples heat-treated at 473, 493, 503 and 513 K under N_2(Figure S3), plots of w_{Fe}, w_{Fe4N}, and w_{amor} *vs.* $t/t_{1/2}$ (Figure S4), experimental data collected under Ar atmosphere (Figure S5 and S6), thermal stability of α"-$Fe_{16}N_2$ (Figure S7), mass spectroscopic data (Figure S8), XRD pattern of the sample heat-treated at 373 K for 14 days under N_2(Figure S9), Rietveld refinement results (Table S1) and $t_{1/2}$ values (Table S2)]. See DOI: 10.1039/b000000x/

1 T. K. Kim, M. Takahashi, *Appl. Phys. Lett.*, 1972, **20**, 492.
2 K. H. Jack, *Proc. R. Soc. A* 1951, **208**, 216.
3 (a) M. Takahashi, H. Shoji, *J. Magn. Magn. Mater*. 2000, **208**, 145; (b) K. Nakajima, S. Okamoto, *Appl. Phys. Lett*. 1990, **56,** 92; (c) M. Komuro, Y. Kozono, N. Hanazono, Y. Sugita, *J. Appl. Phys.*, 1990, **67**, 5126; (d) C. Gao, W. D. Doyle, M. Shamasuzzoha, *J. Appl. Phys*., 1993, **73**, 6579; (e) M. Q. Huang, W. E. Wallace, S. Simizu, S. G. Sankar, *J. Magn. Magn. Mater*. 1994, **135**, 226; (f) H. Jiang, K. Tao, H. Li, *J. Phys. Condens. Mater*. 1994, **6**, L279; (g) C. Ortiz, G. Dumpich, A. H. Morrish, *Appl. Phys. Lett*. 1994, **65**, 2737; (h) X. Bao, R. M. Metzger, M. Carbucicchio, *J. Appl. Phys*. 1994, **75**, 5870; (i) J. M. D. Coey, K. O'Donnel, Q. Qinian, E. Touchais, H. K. Jack, *J. Phys. Condens. Mater*. 1994, **6**, L23; (j) N. Ji, L. F. Alard, E. Lara-Curzio, J.-P. Wang, *Appl. Phys. Lett*. 2011, **98**, 092506; (k) T. Hattori, N. Kamiya, J. Kato, *J. Mag. Soc. Jpn*. 2001, **25**. 927; (l) S. Kikkawa, A. Yamada, Y. Masubuchi, T. Takeda, *Mater. Res. Bull*. 2008, **43**, 3352; (m) K. Shibata, Y. Sasaki, M. Kishimoto, H. Yanagihara, E. Kita, *J. Magn. Soc. Jpn*. 2006, **30**, 501.
4 (a) T. Ogawa, Y. Ogata, R. Gallage, N. Kobayashi, N. Hayashi, Y. Kusano, S. Yamamoto, K. Kohara, M. Doi, M. Takano, M. Takahashi, *Appl. Phys. Express* in press. (b) T. Ogawa, *et al.*, 27-pC-7, The 35th Annual Conference on Magnetics in Japan, 2011. (c) M. Takahashi, *et al.*, AE-01, 56th Annual Conference on Magnetism and Magnetic Material, 2011. (d) M. Takahashi, *et al.*, DD04, IEEE International Magnetic Conference, 2012.
5 Takahashi, M.; Ogawa, T.; Ogata, Y.; Kobayashi, N. P2011-91215A (Japan).
6 A. Sakuma, *J. Appl. Phys.*, 1996, **79**, 5570.
7 (a) Y. Sasaki, N. Usuki, K. Matsuo, M. Kishimoto, *IEEE Trans. Magn*. 2005, **41**, 3241. (b) M. Takahashi, D. Djayaprawira, H. Shoji, *US Patent 6,841,259*. (c)K. Shimba, N. Tezuka, S. Sugimoto, *J. Japan Inst. Metals* 2010, **74**, 209.
8 J. M. D. Coey, *IEEE Trans. Magn*. 2011, **47**, 4671.
9 K. Bourzac, *MIT Technol. Rev*. 2011, **114**, 58.
10 (a) H. Shoji, H. Nashi, K. Eguchi, M. Takahashi, *J. Magn. Magn. Mater*. 1996, **162**, 202; (b) M. Kopcewicz, J. Jagielski, G. Gawlik, A. Turos, *Nucl. Instr. and Meth. in Phys. Res. B* 1992, **B68**, 417; (c) M. Takahashi, H. Shoji, H. Takahashi, T. Wakiyama, *IEEE Trans. Magn.* 1993, **29**, 3040; (d) Y. Xu, E. Hiang, Y. Wang, D. Hou, S. Ren, H. Bai, *Phys. Stat. Sol. (a)* 2001, **184**, 297; (e) M. Takahashi, H. Shoji, H. Takahashi, T. Wakiyama, *J. Appl. Phys.* 1994, **76**, 6642.
11 (a) Y. Sugita, K. Mitsuoka, H. Komuro, Y. Kozono, M. Hanazono, *J. Appl. Phys.* 1991, **70**, 5977; (b) H. Takahashi, M. Komuro, K. Mitsuoka, Y. Sugita, T. Kobayashi, E. Kita, *J. Mag. Soc. Jpn* 1995, **19**, 353.
12 (a) L. Cheng, E. J. Mittemeijer, J. *Metal. Trans. A* 1990, **21**, 13. (b) I. Fall, J.-M.R Genin, *Metal. Mater. Trans. A* 1996, **27A**, 2160.
13 Y. Sugita, K. Mitsuoka, M. Komuro, H. Hoshiya, Y. Kozono, M. Hanazono, *J. Appl. Phys.* 1991, **70**, 5977.
14 A. Khawam, D. R. Flanagan, *J. Phys. Chem. B* 2006, **110**, 17315.
15 F. S. Buffington, K. Hirano, M. Cohen, *Acta Metall*. 1961, **9**, 434.
16 M. Hillert, *Acta Metall*. 1959, **7**, 653.
17 M. Kopcewicz, J. Jagielski, A. Grabias, *J. Appl. Phys.* 1995, **78,** 1312.

Cite this: DOI: 10.1039/c0xx00000x

www.rsc.org/xxxxxx

ARTICLE TYPE

Graphical abstract and short statement of novelty

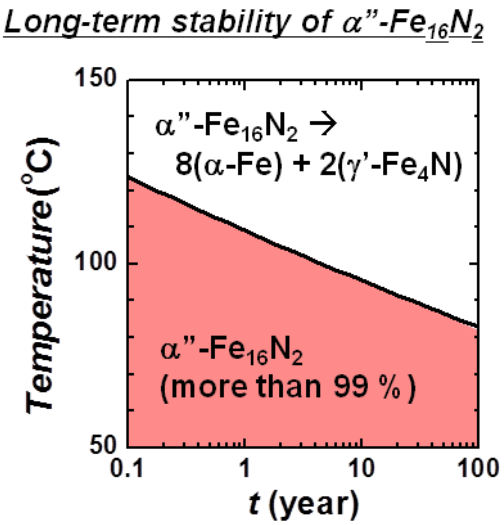

Thermal stability of α"-$Fe_{16}N_2$, which has a large magnetocrystalline anisotropy ($K_u \sim 1 \times 10^7$ erg/cm^3) and saturation magnetization ($M_s \sim 234$ emu/g), though unfortunately thermally unstable, has been *quantitatively* studied.